

Day-Night Asymmetries in Active-Sterile Solar Neutrino Oscillations

H.W. Long¹

Department of Modern Physics, University of Science and
Technology of China, Hefei, Anhui 230026, China

Y.F. Li²

Institute of High Energy Physics, Chinese Academy of
Sciences, Beijing 100049, China

C. Giunti³

INFN, Sezione di Torino, Via P. Giuria 1, I-10125 Torino, Italy

Abstract

Day-night asymmetries in active-sterile solar neutrino oscillations are discussed in the general $3 + N_s$ mixing framework with three active and N_s sterile neutrinos. Analytical expressions of the probability of neutrino flavor transitions in the Earth in the perturbative approximation and in the slab approximation are presented and the effects of active-sterile mixing and of the CP-violating phases are discussed. The accuracy of the analytical approximations and the properties of the day-night asymmetries are illustrated numerically in the 3+1 neutrino mixing framework.

¹E-mail: lhw0128@mail.ustc.edu.cn

²E-mail: liyufeng@ihep.ac.cn

³E-mail: giunti@to.infn.it

1 Introduction

After the measurement of non-zero θ_{13} in recent reactor [1–3] and accelerator [4,5] neutrino experiments, we have a well-established standard framework of three-neutrino oscillations, which explains solar, atmospheric, reactor and accelerator neutrino oscillation data [6] by two distinct mass-squared differences (i.e., Δm_{SOL}^2 and Δm_{ATM}^2) and three non-zero mixing angles (θ_{12} , θ_{23} and θ_{13}). However, there are some short base-line (SBL) neutrino oscillation anomalies that cannot be explained in the three-neutrino mixing framework: the anomalies found in the LSND [7] and MiniBooNE [8] accelerator experiments, the reactor antineutrino anomaly [9] and the Gallium anomaly [10,11]. A neutrino oscillation explanation of these anomalies implies the existence of at least one extra mass-squared difference Δm_{SBL}^2 , such that $\Delta m_{\text{SOL}}^2 \ll \Delta m_{\text{ATM}}^2 \ll \Delta m_{\text{SBL}}^2$, and a small mixing of the three active neutrinos with extra sterile neutrino states [11–14]. Moreover, analyses [15–17] of the data from cosmological observations and Big-Bang Nucleosynthesis may point to the existence of additional dark radiation in the Universe, for which light sterile neutrinos are one of the most promising candidates.

The existence of light sterile neutrinos and their mixing with the standard active neutrinos can be tested also by studying their effects in solar [18–22] and atmospheric [23] neutrino oscillations, as well as in the processes of the beta decay [24,25] and neutrinoless double beta decay [26]. In this paper we discuss the possible effects of active-sterile mixing on the day-night asymmetries of solar neutrino oscillations.

Solar neutrinos are produced in the core of the Sun and undergo the large-mixing-angle (LMA) Mikheev-Smirnov-Wolfenstein (MSW) mechanism [27,28] before they propagate out of the solar surface. This mechanism was established about ten years ago after the decisive evidences in favor of solar neutrino oscillations obtained in the SNO [29] and KamLAND [30] experiments. Since then, testing the MSW mechanism with low energy solar neutrinos [31] and searching for sub-leading effects [18–21] beyond the standard three-neutrino oscillation have become the central concern of solar neutrino searches. Moreover, the terrestrial matter effect in terms of the regeneration effects and day-night asymmetries [32] of solar neutrino oscillations can give direct and independent tests of the MSW mechanism and constrain different kinds of sub-leading effects. Different calculations of the day-night asymmetries in the three-neutrino mixing scheme have been discussed in the recent literature [33–36]. In this work we extend the discussion to the general framework with three active and N_s sterile neutrinos (the $3 + N_s$ scheme). In this study, we derive the analytical expressions of the day-night asymmetries in the $3 + N_s$ mixing scheme without any constraint on the mixing elements, assuming only a realistic hierarchy on the mass-squared differences. Calculations using both the perturbative approximation and the slab approximation are checked by comparing their results with those of accurate numerical calculations.

The outline of this work is planned as follows. In Section 2 we review briefly the general framework of neutrino evolution in matter and present the neutrino oscillation probabilities relevant to the experimental results in the daytime [19]. In Section 3 we calculate the oscillation probabilities in the nighttime for solar neutrinos propagating inside the Earth before being detected, and we discuss the calculation of the day-night asymmetries by using different approximation methods. In Section 4 we test the accuracy of our analytical calculations in different approximations comparing the results with those

obtained with an accurate numerical solution of the solar neutrino evolution inside the Earth. We also illustrate the properties of the day-night asymmetries using the analytical approximations. Finally, we conclude in Section 5 and we present in the Appendices additional details of the calculations and the parametrization of the four-neutrino mixing matrix that we use in the examples.

2 Oscillations from the Sun to Earth

In this Section, we review the general framework in Ref. [19] of the neutrino evolution in matter and the solar neutrino oscillation probabilities in the daytime.

To begin with, the evolution of solar neutrinos propagating in matter (in the Sun or in the Earth) is described by the MSW equation [27, 28]

$$i \frac{d}{dx} \Psi = (UMU^\dagger + \mathcal{V}) \Psi \quad , \quad (1)$$

where $\Psi = (\psi_e, \psi_\mu, \psi_\tau, \psi_{s_1}, \dots, \psi_{s_{N_s}})^T$ is the flavor transition amplitudes, U is the $(3 + N_s) \times (3 + N_s)$ neutrino mixing matrix, and

$$\mathcal{M} = \text{diag} \left(0, \frac{\Delta m_{21}^2}{2E}, \frac{\Delta m_{31}^2}{2E}, \frac{\Delta m_{41}^2}{2E}, \dots, \frac{\Delta m_{N1}^2}{2E} \right) \quad , \quad (2)$$

$$\mathcal{V} = \text{diag}(V_{\text{CC}} + V_{\text{NC}}, V_{\text{NC}}, V_{\text{NC}}, 0, \dots, 0) \quad , \quad (3)$$

where E is the neutrino energy and $\Delta m_{kj}^2 = m_k^2 - m_j^2$ are the mass-squared differences. The charge-current (CC) and neutral-current (NC) neutrino matter potentials in Eq. (3) are defined as

$$V_{\text{CC}} = \sqrt{2} G_{\text{F}} N_e \simeq 7.63 \times 10^{-14} \frac{N_e}{N_{\text{A}} \text{ cm}^{-3}} \text{ eV} \quad , \quad V_{\text{NC}} = -\frac{1}{2} \sqrt{2} G_{\text{F}} N_n \quad , \quad (4)$$

where G_{F} is the Fermi constant, N_e and N_n are the electron and neutron number densities respectively, and N_{A} is the Avogadro's number. In a neutral medium, we can use the electron fraction

$$Y_e = \frac{N_e}{N_e + N_n} \quad , \quad (5)$$

to define the ratio R_{NC} of matter potentials as

$$V_{\text{NC}} = R_{\text{NC}} V_{\text{CC}} \quad , \quad \text{with} \quad R_{\text{NC}} = -\frac{1 - Y_e}{2Y_e} \quad . \quad (6)$$

In the vacuum mass basis $\Psi^{\text{V}} = (\psi_1^{\text{V}}, \dots, \psi_N^{\text{V}})^T = U^\dagger \Psi$, the flavor transitions generated by Δm_{21}^2 are decoupled from those generated by the larger mass-squared differences, because of the hierarchy

$$V_{\text{CC}} \sim |V_{\text{NC}}| \lesssim \frac{\Delta m_{21}^2}{2E} \ll \frac{|\Delta m_{k1}^2|}{2E} \quad \text{for} \quad k \geq 3 \quad , \quad (7)$$

for solar and terrestrial matter densities. Therefore, the full neutrino evolution equation in Eq. (1) can be truncated to a 2×2 evolution equation

$$i \frac{d}{dx} \Psi_2^{\text{V}} = \mathcal{H}_2^{\text{V}} \Psi_2^{\text{V}} \quad , \quad (8)$$

with $\Psi_2^V = (\psi_1^V, \psi_2^V)^T$ and

$$\mathcal{H}_2^V = \begin{pmatrix} -\delta + V \cos 2\xi & V \sin 2\xi e^{i\varphi} \\ V \sin 2\xi e^{-i\varphi} & \delta - V \cos 2\xi \end{pmatrix} . \quad (9)$$

All the other amplitudes evolve independently as

$$\psi_k^V(x) \simeq \psi_k^V(0) \exp\left(-i \frac{\Delta m_{k1}^2 x}{2E}\right) , \quad \text{for } k \geq 3 . \quad (10)$$

The vacuum oscillation wave number δ , the effective potential V , the matter-dependent mixing angle ξ and the complex phase φ are defined respectively as

$$\delta = \frac{\Delta m_{12}^2}{4E} , \quad (11)$$

$$V = \frac{1}{2} V_{\text{CC}} \sqrt{X^2 + |Y|^2} , \quad (12)$$

$$\xi = \frac{1}{2} \arctan \frac{|Y|}{X} , \quad (13)$$

$$\varphi = \arg(Y) , \quad (14)$$

with

$$X = |U_{e1}|^2 - |U_{e2}|^2 - R_{\text{NC}} \sum_{i=1}^{N_s} (|U_{s_i1}|^2 - |U_{s_i2}|^2) , \quad (15)$$

$$Y = 2 \left(U_{e1}^* U_{e2} - R_{\text{NC}} \sum_{i=1}^{N_s} U_{s_i1}^* U_{s_i2} \right) . \quad (16)$$

We can define an effective mass basis in matter for the two-neutrino framework in Eq. (8) as

$$\Psi_2^V = W_2(\omega, \varphi) \Psi_2^M , \quad (17)$$

where $\Psi_2^M = (\psi_1^M, \psi_2^M)^T$ is the amplitude vector in the effective mass basis, and

$$W_2(\omega, \varphi) \equiv \begin{pmatrix} \cos \omega & \sin \omega e^{i\varphi} \\ -\sin \omega e^{-i\varphi} & \cos \omega \end{pmatrix} , \quad (18)$$

with

$$\tan 2\omega = \frac{V \sin 2\xi}{\delta - V \cos 2\xi} , \quad (19)$$

is the unitary matrix which diagonalizes the Hamiltonian in Eq. (9). The evolution equation in the effective mass basis in matter is

$$i \frac{d}{dx} \Psi_2^M = \mathcal{H}_2^M \Psi_2^M , \quad (20)$$

where the Hamiltonian is given by

$$\begin{aligned} \mathcal{H}_2^{\text{M}} &= \mathcal{H}_{\text{ad}}^{\text{M}} + \mathcal{H}_{\text{na}}^{\text{M}} \\ &\equiv \begin{pmatrix} -\delta_{\text{M}} & 0 \\ 0 & \delta_{\text{M}} \end{pmatrix} + \begin{pmatrix} -\dot{\varphi} \sin^2 \omega & (\frac{1}{2}\dot{\varphi} \sin 2\omega - i\dot{\omega})e^{i\varphi} \\ (\frac{1}{2}\dot{\varphi} \sin 2\omega + i\dot{\omega})e^{-i\varphi} & \dot{\varphi} \sin^2 \omega \end{pmatrix} , \end{aligned} \quad (21)$$

with

$$\delta_{\text{M}} = \sqrt{(\delta - V \cos 2\xi)^2 + (V \sin 2\xi)^2} , \quad (22)$$

$$\dot{\varphi} \equiv \frac{d\varphi}{dx} , \quad \dot{\omega} \equiv \frac{d\omega}{dx} . \quad (23)$$

Note that we have decomposed the Hamiltonian into the adiabatic (ad) and non-adiabatic (na) parts in Eq. (21), which take into account the dependence of ω and φ on the variable matter density along the neutrino propagation path.

To proceed, we define a parametrization [18] of the neutrino mixing matrix U as

$$\begin{cases} U_{\beta 1} = \cos \theta_{\beta} \cos \chi_{\beta} e^{i\phi_{\beta 1}} \\ U_{\beta 2} = \sin \theta_{\beta} \cos \chi_{\beta} e^{i\phi_{\beta 2}} \end{cases} \quad \text{with} \quad \cos^2 \chi_{\beta} = |U_{\beta 1}|^2 + |U_{\beta 2}|^2 , \quad (24)$$

and a formal solution of the averaged amplitudes for solar neutrino evolution as

$$\begin{cases} \overline{|\psi_1^{\text{M}}(x_d)|^2} = |\psi_1^{\text{M}}(0)|^2 (1 - P_{12}) + |\psi_2^{\text{M}}(0)|^2 P_{12} \\ \overline{|\psi_2^{\text{M}}(x_d)|^2} = |\psi_1^{\text{M}}(0)|^2 P_{12} + |\psi_2^{\text{M}}(0)|^2 (1 - P_{12}) \end{cases} , \quad (25)$$

where x_d is the coordinate of the detector on the Earth, P_{12} is the level-crossing probability generated by the off-diagonal non-adiabatic terms in Eq. (21) between ψ_1^{M} and ψ_2^{M} during their propagation inside the Sun.

Finally, we obtain the averaged solar neutrino oscillation probabilities in the daytime (see Ref. [19] for a careful derivation) as

$$\overline{P}_{\nu_e \rightarrow \nu_{\beta}}^{\text{S}} = \cos^2 \chi_e \cos^2 \chi_{\beta} \overline{P}_{\nu_e \rightarrow \nu_{\beta}}^{(2\nu)} + \sum_{k=3}^N |U_{ek}|^2 |U_{\beta k}|^2 , \quad (26)$$

where

$$\overline{P}_{\nu_e \rightarrow \nu_{\beta}}^{(2\nu)} = \frac{1}{2} + \left(\frac{1}{2} - P_{12}\right) \cos 2\Theta_e^0 \cos 2\theta_{\beta} , \quad (27)$$

$$\cos 2\Theta_e^0 = \cos 2\theta_e \cos 2\omega^0 - \cos \Phi_e^0 \sin 2\theta_e \sin 2\omega^0 , \quad (28)$$

$$\Phi_e^0 = \phi_{e1} - \phi_{e2} + \varphi^0 , \quad (29)$$

and all the parameters with a ‘0’ superscript are defined at the neutrino production point.

3 Day-Night Asymmetries

In Section 2 we have briefly reviewed the derivation of the solar neutrino oscillation probabilities (26) in the daytime. However, solar neutrino fluxes might be affected by the Earth’s matter if they are detected at night and travel inside the Earth before detection

(the so-called “regeneration effect”). Therefore, there can be measurable differences of the oscillation probabilities in the daytime and nighttime which can be quantified by defining suitable day-night asymmetries. In the standard framework of three-neutrino mixing, there is only a single day-night asymmetry for the electron neutrino survival probability [33–36]. In the general $3 + N_s$ mixing scheme with three active and N_s sterile neutrinos which we consider there is an additional asymmetry for the electron-to-sterile neutrino transition probability, which can be revealed by precise neutral-current measurements.

Because of the spread of the solar neutrino production areas and finite detector energy resolution, the contributions of the different mass eigenstates to the oscillation probabilities are incoherent [37]. Therefore, the oscillation probabilities without [crossing only the Sun (S)] and with [crossing both the Sun (S) and the Earth (E)] the terrestrial matter effects are given, respectively, by¹

$$\overline{P}_{\nu_e \rightarrow \nu_\beta}^S = \sum_{k=1}^{3+N_s} P_{\nu_e \rightarrow \nu_k}^S P_{\nu_k \rightarrow \nu_\beta}^V, \quad (30)$$

$$\overline{P}_{\nu_e \rightarrow \nu_\beta}^{SE} = \sum_{k=1}^{3+N_s} P_{\nu_e \rightarrow \nu_k}^S P_{\nu_k \rightarrow \nu_\beta}^E, \quad (31)$$

where

$$P_{\nu_2 \rightarrow \nu_\beta}^V = |U_{\beta 2}|^2 = \sin^2 \theta_\beta \cos^2 \chi_\beta, \quad (32)$$

is the transition probability between ν_k and ν_β in vacuum. From Eq. (10), we obtain

$$P_{\nu_e \rightarrow \nu_k}^S \simeq |U_{ek}|^2, \quad P_{\nu_k \rightarrow \nu_\beta}^E \simeq |U_{\beta k}|^2, \quad (k \geq 3), \quad (33)$$

and due to the unitarity of oscillation probabilities, we have the following relations

$$P_{\nu_e \rightarrow \nu_1}^S = 1 - \sum_{k=3}^{3+N_s} |U_{ek}|^2 - P_{\nu_e \rightarrow \nu_2}^S, \quad (34)$$

$$P_{\nu_1 \rightarrow \nu_\beta}^E = 1 - \sum_{k=3}^{3+N_s} |U_{\beta k}|^2 - P_{\nu_2 \rightarrow \nu_\beta}^E. \quad (35)$$

By using the above relations and the probabilities in Eq. (26), we obtain the neutrino oscillation probabilities including the terrestrial matter effects as follows:

$$\begin{aligned} \overline{P}_{\nu_e \rightarrow \nu_\beta}^{SE} &= \overline{P}_{\nu_e \rightarrow \nu_\beta}^S + \left(P_{\nu_2 \rightarrow \nu_\beta}^E - P_{\nu_2 \rightarrow \nu_\beta}^V \right) \\ &\times \left\{ \frac{(|U_{e1}|^2 + |U_{e2}|^2)(|U_{\beta 1}|^2 + |U_{\beta 2}|^2) - 2(\overline{P}_{\nu_e \rightarrow \nu_\beta}^S - \sum_{k=3}^N |U_{ek}|^2 |U_{\beta k}|^2)}{|U_{\beta 1}|^2 - |U_{\beta 2}|^2} \right\}. \end{aligned} \quad (36)$$

Using Eqs. (25), (26) and (27), this expression can be written as²

$$\overline{P}_{\nu_e \rightarrow \nu_\beta}^{SE} = \overline{P}_{\nu_e \rightarrow \nu_\beta}^S - \cos^2 \chi_e (1 - 2P_{12}) \cos 2\Theta_e^0 R_{2\beta}, \quad (37)$$

¹ Some aspects of the terrestrial matter effects in the case of four-neutrino mixing have been already discussed in Refs. [20, 38, 39].

²From the discussion in Ref. [19], we know that P_{12} is negligibly small in the Sun. Therefore, we neglect it in the numerical discussion in Section 4.

where

$$R_{2\beta} = P_{\nu_2 \rightarrow \nu_\beta}^E - P_{\nu_2 \rightarrow \nu_\beta}^V \quad , \quad (38)$$

are the regeneration factors of active-sterile solar neutrino oscillations.

It is convenient to define the day-night asymmetries of the oscillation probabilities

$$D_{e\beta} = \overline{P}_{\nu_e \rightarrow \nu_\beta}^{\text{SE}} - \overline{P}_{\nu_e \rightarrow \nu_\beta}^{\text{S}} = -\cos^2 \chi_e (1 - 2P_{12}) \cos 2\Theta_e^0 R_{2\beta} \quad , \quad (39)$$

which depend on the mixing parameter χ_e , on the solar oscillations quantities P_{12} and Θ_e^0 , and on the regeneration factors $R_{2\beta}$ in the Earth.

Note that, taking into account the unitarity of probabilities, the measurable event rates in solar experiments depend on two independent regeneration factors: R_{2e} and R_{2s} . To count the number of relevant mixing angles and CP-violating phases in the regeneration factors, we can employ the same arguments presented in Ref. [19]. Because of the freedom in the complex rotations of the ν_μ - ν_τ sector and among the sterile neutrino flavors, the probability $P_{\nu_2 \rightarrow \nu_\beta}^E$ depends on $3N_s+2$ mixing angles and $2N_s$ Dirac CP-violating phases. In order to express the regeneration factors and the oscillation probabilities in terms of this minimal number of oscillation parameters, it is necessary to choose a convenient parameterization of the mixing matrix. However, considering for example the 3+1 mixing scheme, it is interesting to study the information that solar neutrino measurements can give on the elements U_{e4} , $U_{\mu 4}$ and $U_{\tau 4}$ of the mixing matrix, which quantify the mixing of active and sterile neutrinos. Therefore, it is convenient to use the parametrization of U in Eq. (87), in which U_{e4} , $U_{\mu 4}$ and $U_{\tau 4}$ are proportional, respectively, to the sines of the mixing angles θ_{14} , θ_{24} and θ_{34} and $U_{\mu 4}$ and $U_{\tau 4}$ are directly related, respectively, to the CP-violating phases η_{24} and η_{34} [see Eqs. (90) and (95)]. In this case, the regeneration factors and the oscillation probabilities depend on all the six mixing angles and the three CP-violating phases in Appendix B³.

The regeneration factors are determined by the transition probabilities $P_{\nu_2 \rightarrow \nu_\beta}^E$ inside the Earth. By using Eqs. (10) and (24) and the initial condition $\psi_k^V(x_i) = \delta_{k2}$, we obtain the formal expression

$$\begin{aligned} P_{\nu_2 \rightarrow \nu_\beta}^E(x_d) &= |\psi_\beta(x_d)|^2 = |U_{\beta 1} \psi_1^V(x_d) + U_{\beta 2} \psi_2^V(x_d)|^2 \\ &= \frac{1}{2} \cos^2 \chi_\beta \left\{ 1 + \cos 2\theta_\beta (|\psi_1^V(x_d)|^2 - |\psi_2^V(x_d)|^2) \right. \\ &\quad + 2 \sin 2\theta_\beta \cos(\phi_{\beta 2} - \phi_{\beta 1}) \text{Re}(\psi_1^{V*}(x_d) \psi_2^V(x_d)) \\ &\quad \left. - 2 \sin 2\theta_\beta \sin(\phi_{\beta 2} - \phi_{\beta 1}) \text{Im}(\psi_1^{V*}(x_d) \psi_2^V(x_d)) \right\} \quad , \quad (40) \end{aligned}$$

where the amplitudes in the vacuum mass basis $\psi_i^V(x_d)$ with $(i = 1, 2)$ can be calculated using the evolution equation inside the Earth.

The most accurate calculation of the oscillation probabilities can be obtained with a numerical solution of the evolution equation (8), using a precise density profile of matter in the Earth. However, such a numerical solution is too time-consuming if one wants

³ The mixing angles and CP-violating phases of the appropriate parameterization in which the regeneration factors and the oscillation probabilities depend on only five mixing angles and two CP-violating phases are complicated functions of the mixing parameters in Appendix B.

to explore a large volume of the space of the mixing-parameters and often one needs analytic expressions for the oscillation probabilities in order to study their properties. Therefore, in the following two subsections, we describe two different approximations which allow us to obtain analytical expressions of $P_{\nu_2 \rightarrow \nu_\beta}^E$. We discuss the accuracy of these approximations in Section 4.

3.1 Perturbative Approximation

For the density profile inside the Earth, the matrix elements of the non-adiabatic Hamiltonian in Eq. (21) are much smaller than those of the adiabatic Hamiltonian and can be treated as a perturbation. This is due to the fact that the effective potential V itself can be treated as a perturbation, because $V \ll \Delta m_{21}^2/2E$. Therefore, both ω and $\dot{\omega}$ are small, even at the boundaries of two adjacent shells in the Earth where there are sudden changes of the matter density.

In the S -matrix formalism, the neutrino evolution can be written formally as

$$\Psi_2^B(x_f) = S^B(x_f, x_i) \Psi_2^B(x_i) \quad , \quad (41)$$

where the superscript denotes the mass basis in vacuum ($B = V$) or in matter ($B = M$), and x_i and x_f are the initial and final points of the neutrino trajectory. The two S -matrices in the vacuum and matter mass bases are connected by the transformation

$$S^V(x_f, x_i) = W_2(\omega_f, \varphi_f) S^M(x_f, x_i) W_2^\dagger(\omega_i, \varphi_i) \quad , \quad (42)$$

with $W_2(\omega, \varphi)$ given in Eq. (18).

We can calculate the S -matrix in the mass basis in matter using the general perturbation theory (see Refs. [40, 41] for details):

$$\begin{aligned} S^M(x_f, x_i) &\simeq S_{\text{ad}}^M(x_f, x_i) - i S_{\text{ad}}^M(x_f, x_i) \int_{x_i}^{x_f} S_{\text{ad}}^M(x, x_i)^{-1} \mathcal{H}_{\text{na}}^M(x) S_{\text{ad}}^M(x, x_i) dx \\ &= S_{\text{ad}}^M(x_f, x_i) - i S_{\text{ad}}^M(x_f, x_i) \begin{pmatrix} -A & C \\ C^* & A \end{pmatrix} \\ &= \begin{pmatrix} (1 + iA)e^{i\Delta} & -iC e^{i\Delta} \\ -iC^* e^{-i\Delta} & (1 - iA)e^{-i\Delta} \end{pmatrix} \quad , \end{aligned} \quad (43)$$

with

$$\begin{aligned} S_{\text{ad}}^M(x_f, x_i) &= \exp\left\{-i \int_{x_i}^{x_f} \mathcal{H}_{\text{ad}}^M(x) dx\right\} \\ &= \begin{pmatrix} e^{i\Delta(x_f, x_i)} & 0 \\ 0 & e^{-i\Delta(x_f, x_i)} \end{pmatrix} \quad , \end{aligned} \quad (44)$$

$$\Delta(x_f, x_i) = \int_{x_i}^{x_f} \delta_M dx \quad , \quad (45)$$

$$A(x_f, x_i) = \int_{x_i}^{x_f} \dot{\varphi} \sin^2 \omega dx \quad , \quad (46)$$

$$C(x_f, x_i) = \int_{x_i}^{x_f} \left(\frac{1}{2} \dot{\varphi} \sin 2\omega - i\dot{\omega}\right) e^{i[\varphi - 2\Delta(x, x_i)]} dx \quad . \quad (47)$$

Since the matter effects at the boundaries (i.e., x_i and x_f) of the neutrino path inside the Earth are negligible, we have $W(\omega_i, \varphi_i) = W(\omega_f, \varphi_f) = 1$ and $S^V(x_f, x_i) = S^M(x_f, x_i)$. Therefore, as shown in Appendix A.1, the transition probability $P_{\nu_2 \rightarrow \nu_\beta}^E$ can be approximated to the first order of A and C as

$$\begin{aligned} P_{\nu_2 \rightarrow \nu_\beta}^E(x_f) &\simeq P_{\nu_2 \rightarrow \nu_\beta}^V + \cos^2 \chi_\beta \sin 2\theta_\beta \text{Im} [C e^{i(2\Delta + \phi_{\beta 1} - \phi_{\beta 2})}] \\ &= P_{\nu_2 \rightarrow \nu_\beta}^V + \cos^2 \chi_\beta \sin 2\theta_\beta \text{Im} \left\{ \int_{x_i}^{x_f} \left(\frac{1}{2} \dot{\varphi} \sin 2\omega - i\dot{\omega} \right) e^{i[2\Delta(x_f, x) + \Phi_\beta]} dx \right\}, \quad (48) \end{aligned}$$

where $\Phi_\beta = \phi_{\beta 1} - \phi_{\beta 2} + \varphi$. Notice that Φ_β is invariant under the rephasing transformation of $U_{\alpha k} \rightarrow e^{i\varphi_\alpha} U_{\alpha k} e^{i\varphi_k}$, and gives the intrinsic phase-dependence of the day-night asymmetries. Furthermore, as shown in Appendix A.1, in the approximation of a constant electron fraction Y_e [43] (i.e., $\dot{\varphi} = 0$), the transition probability $P_{\nu_2 \rightarrow \nu_\beta}^E$ can be further simplified to the first order of V as

$$P_{\nu_2 \rightarrow \nu_\beta}^E(x_f) \simeq P_{\nu_2 \rightarrow \nu_\beta}^V + \cos^2 \chi_\beta \sin 2\theta_\beta \sin 2\xi \int_{x_i}^{x_f} V(x) \sin [2\Delta(x_f, x) + \Phi_\beta] dx. \quad (49)$$

In Appendix A.3 we derive the limit of this expression for $P_{\nu_2 \rightarrow \nu_e}^E(x_f)$ in the case of vanishing active-sterile mixing in order to show that it agrees with that presented in the case of standard three-neutrino mixing in Ref. [34].

In Section 4 we will show that the perturbative approximation gives an accurate description of neutrino evolution inside the Earth. However, since the integrations in Eqs. (48) and (49) are very time-consuming, it is useful to investigate if there are other approximate methods which give accurate and more rapid solutions of the evolution equation. In the next subsection we discuss the analytical calculation of $P_{\nu_2 \rightarrow \nu_\beta}^E$ in the slab approximation.

3.2 Slab Approximation

In the slab approximation, the radial symmetric profile of the matter density inside the Earth is divided into N shells ($1 \leq i \leq N$, where $i = 1$ is the innermost shell), such that the density variation is very small within each shell and sudden changes happen at the boundaries (the biggest change happens at the mantle-core boundary).

When a solar neutrino travels inside the Earth, the neutrino trajectory crosses the outer n shells ($n \leq N$) of the Earth and contains $2n - 1$ segments with constant density. The number n and the lengths of the segments depend on the nadir angle of the trajectory, which ends at the detector. We denote the coordinates of the segment boundaries as $x_{-n}, x_{-n+1}, \dots, x_{-1}, x_0, x_1, \dots, x_{n-1}, x_n$, starting from the beginning of the first segment at x_{-n} where the neutrino enters the Earth and following the neutrino path until it reaches the detector at x_n . For convenience, we have define a point x_0 at the middle point of the trajectory, which artificially splits in two equal parts the segment of the trajectory in the $(N - n + 1)$ -th shell. In this way, there are two segments with equal length in each shell: in the $(N - n + k)$ -th shell, with $k = 1, \dots, n$, the two segments have boundaries (x_{-k}, x_{-k+1}) and (x_{k-1}, x_k) .

In each segment of the trajectory the electron fraction Y_e , the CC potential V_{CC} and the induced parameters ξ , φ , ω , V and δ_M are constant. Due to the radial symmetry of

the Earth, we have $X_k = X_{-k}$ for $X = \xi, \varphi, \omega, V, \delta_M$. Since the matrix elements of the non-adiabatic Hamiltonian $\mathcal{H}_{\text{na}}^M$ of Eq. (21) vanish in each segment and δ_M is constant, we obtain

$$\begin{aligned} S^M(x_k, x_{k-1}) &\simeq \exp\left\{-i \int_{x_i}^{x_f} \mathcal{H}_{\text{ad}}^M dx\right\} \\ &= \text{diag}\{e^{i\delta_M(x_k - x_{k-1})}, e^{-i\delta_M(x_k - x_{k-1})}\} \equiv S^M(x_k - x_{k-1}) \quad , \end{aligned} \quad (50)$$

and accordingly

$$S^V(x_k, x_{k-1}) = [W(\omega, \varphi) S^M(\Delta x_k) W^\dagger(\omega, \varphi)]_{(k)} \equiv S_k^V \quad , \quad (51)$$

where $\Delta x_k = x_k - x_{k-1}$ and the subscript (k) indicates the $(N - n + k)$ -th shell. Since $\Psi_2^V(x_k) = S_k^V \Psi_2^V(x_{k-1})$, the evolution inside the Earth is given recursively by

$$\Psi_2^V(x_n) \simeq S_{\text{slab}}^V \Psi_2^V(x_{-n}) \quad , \quad (52)$$

with

$$\begin{aligned} S_{\text{slab}}^V &= S_n^V S_{n-1}^V \dots S_1^V S_{-1}^V \dots S_{-(n-1)}^V S_{-n}^V \\ &= S_n^V S_{n-1}^V \dots S_1^V S_1^V \dots S_{n-1}^V S_n^V \quad . \end{aligned} \quad (53)$$

Note that there are two S_1^V in Eq. (53) because we have divided the innermost segment into two connected ones with the central point x_0 . By using Eqs. (40), (52) and (53), we can calculate the transition probability $P_{\nu_2 \rightarrow \nu_\beta}^E$ in a self-consistent way. This method is usually adopted in the data analysis of solar neutrino experiments, because it is much more rapid and efficient than the perturbation method.

Employing the perturbative approximation for the effective potential V , we can further simplify the transition probability $P_{\nu_2 \rightarrow \nu_\beta}^E$ to the first order of V_k as

$$\begin{aligned} P_{\nu_2 \rightarrow \nu_\beta}^E(x_n) &\simeq P_{\nu_2 \rightarrow \nu_\beta}^V + \cos^2 \chi_\beta \sin 2\theta_\beta \times \\ &\sum_{k=1}^n \frac{V_k}{\delta} \sin 2\xi_k \sin(\delta L_n + \Phi_{\beta(k)}) (\sin \delta L_k - \sin \delta L_{k-1}) \quad , \end{aligned} \quad (54)$$

where L_k is the length of the trajectory inside the outer boundary of the $(N - n + k)$ -th shell:

$$L_k = x_k - x_{-k} \quad . \quad (55)$$

The derivation of this expression is described in details in Appendix A.2. We also derive in Appendix A.3 the limit in the case of vanishing active-sterile mixing of the expression (54) for the transition probability $P_{\nu_2 \rightarrow \nu_e}^E$, in order to show that it agrees with that derived in the case of standard three-neutrino mixing in Ref. [35].

Finally, let us discuss the dependence in $P_{\nu_2 \rightarrow \nu_\beta}^E$ and $R_{2\beta}$ on the mixing parameters. From Eqs. (49) and (54), one can see that the regeneration factors are explicitly proportional to the mixing parameters $\cos^2 \chi_\beta$ and $\sin 2\theta_\beta$. Moreover, the effective potential V , the effective mixing angle ξ and the oscillation wave number in matter δ_M take part in the regeneration factors via the integration or summation of the contributions in the whole trajectory inside the Earth. The most distinct property in $P_{\nu_2 \rightarrow \nu_\beta}^E$ is the explicit dependence on the CP-violating phases Φ_β , which contribute to the oscillating phases.

i	Shell	$[r_{i-1}, r_i]$	$[\cos \kappa_{N i-1}, \cos \kappa_{N i}]$	α_i	β_i	γ_i	$\bar{N}_{e i}$	$Y_{e i}$
1	Inner core	[0, 0.192]	[1, 0.98]	6.099	-4.119	0.000	6.048	0.466
2	Outer core	[0.192, 0.546]	[0.98, 0.84]	5.803	-3.653	-1.086	5.209	0.466
3	Lower mantle	[0.546, 0.895]	[0.84, 0.45]	3.156	-1.459	0.280	2.468	0.494
4	Transition Zone	[0.895, 0.937]	[0.45, 0.35]	-5.376	19.210	-12.520	1.922	0.494
5	Upper mantle	[0.937, 1]	[0.35, 0]	11.540	-20.280	10.410	1.689	0.494

Table 1: Descriptions of the simplified PREM model with five shells. The shell names and the values of the coefficients are quoted from Table 1 of Ref. [43] (see text for details).

4 Numerical Discussion

In the previous Section we have obtained in Eqs. (49), (52) and (54) three approximate analytical expressions for the transition probability $P_{\nu_2 \rightarrow \nu_\beta}^E$. We will call them, respectively, the perturbative approximation (PERT), the slab approximation (SLAB) and the slab plus perturbative approximation (SLAB+PERT). In this Section, we are going to test the accuracy of these analytical approximations in the case of 3 + 1 mixing and discuss the main properties of the corresponding day-night asymmetries.

First of all, in order to calculate the neutrino evolution inside the Earth we need an accurate description of the density profile of the Earth. In our calculations, we employ a simplified version of the preliminary Earth reference model (PREM) [42], which contains [43] five shells and uses the polynomial function

$$N_i(r) = \alpha_i + \beta_i r^2 + \gamma_i r^4 \quad , \quad (56)$$

for the i -th shell ($1 \leq i \leq 5$, where $i = 1$ is the innermost shell) to describe the Earth's density at the radial distance r . The values of the coefficients are given in Table 1, which gives also the averaged electron density $\bar{N}_{e i}$ in the i -th shell, which will be used in the slab approximation. The electron fractions Y_e are also provided for the core and mantle regions. The cosine values of the nadir angle κ_N corresponding to the radial boundaries $[r_{i-1}, r_i]$ of each shell are given in the form $[\cos \kappa_{N i-1}, \cos \kappa_{N i}]$. We employ the fourth-order Runge-Kutta method for the numerical solution of the neutrino evolution equation in the Earth, using the density matrix formalism (see Appendix C of Ref. [19] for a detailed introduction). Finally, in Appendix B we give the explicit parametrization of U and the values of the oscillation parameters used in our examples.

In Figs. 1 and 2, we check the accuracy of the three analytical approximations by drawing the regeneration factors $R_{2\beta}$ (i.e., R_{2e} and R_{2s}) as functions of the nadir angle, for a neutrino energy of $E = 10$ MeV. The three upper panels show the comparison of the result of each analytical approximation (PERT, SLAB and SLAB+PERT from top to bottom) with that of the numerical calculation. In the lowermost panels we have drawn the differences between the analytical and numerical results as functions of the nadir angle.

From Figs. 1 and 2, we observe that the PERT approximation gives an accurate description of the solar neutrino evolution inside the Earth, even for the neutrino trajectories crossing the core (i.e. for $\cos \kappa_N \gtrsim 0.84$). One can also see that the SLAB approximation gives the correct frequencies of the oscillatory behavior of R_{2e} and R_{2s} , but there are significant differences in the oscillating amplitudes with respect to those obtained with the numerical calculation for neutrinos crossing the core. However, as we

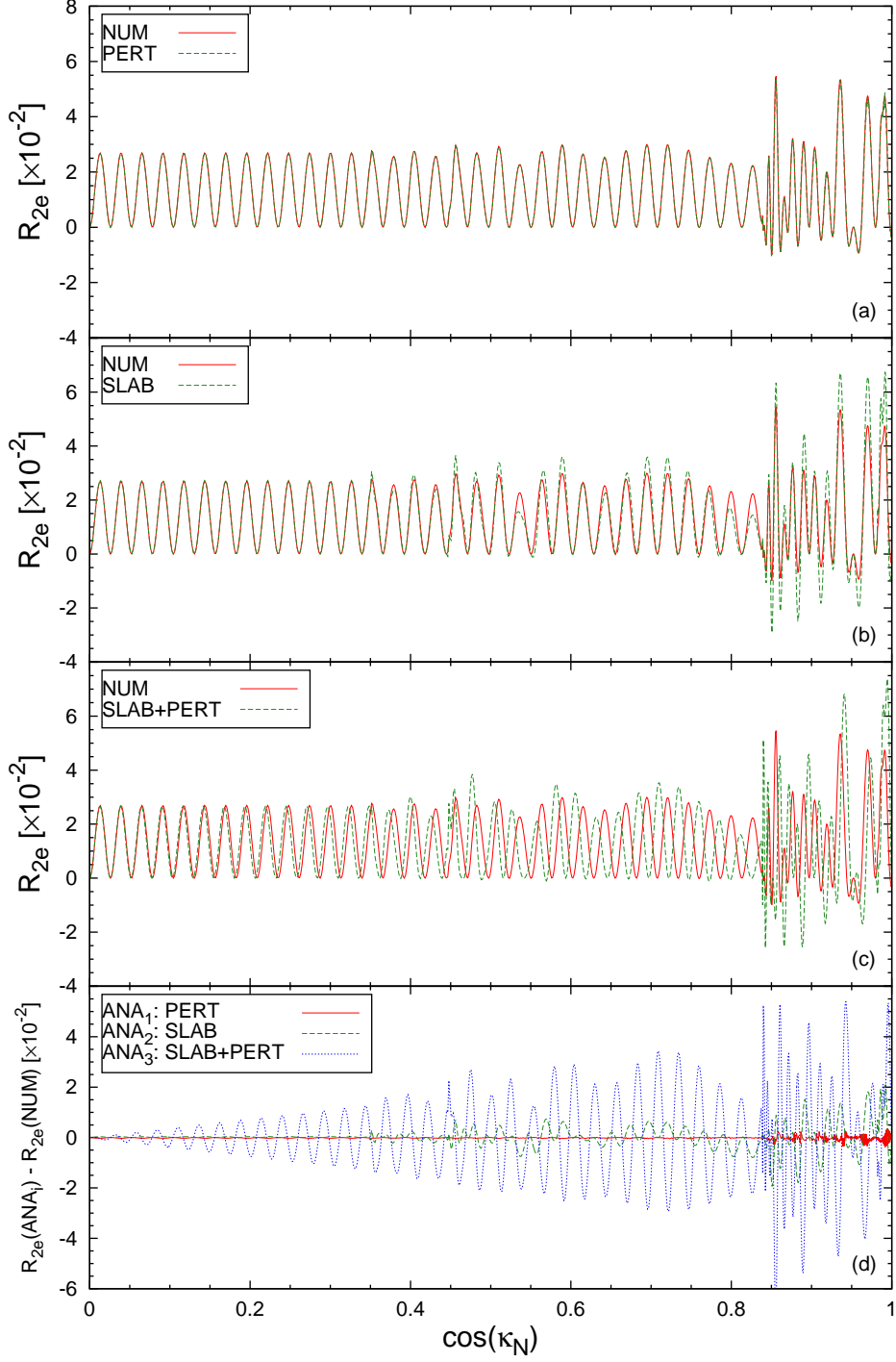


Figure 1: Comparisons of the numerical calculation of the regeneration factor R_{2e} as the function of the nadir angle with the corresponding analytical ones in the PERT, SLAB and SLAB+PERT approximations, respectively. The lowermost panel is illustrated with the three differences between the numerical and analytical results. The neutrino energy is fixed to 10 MeV. All the oscillation parameters are set to M1 and P1 in Eqs. (96) and (97).

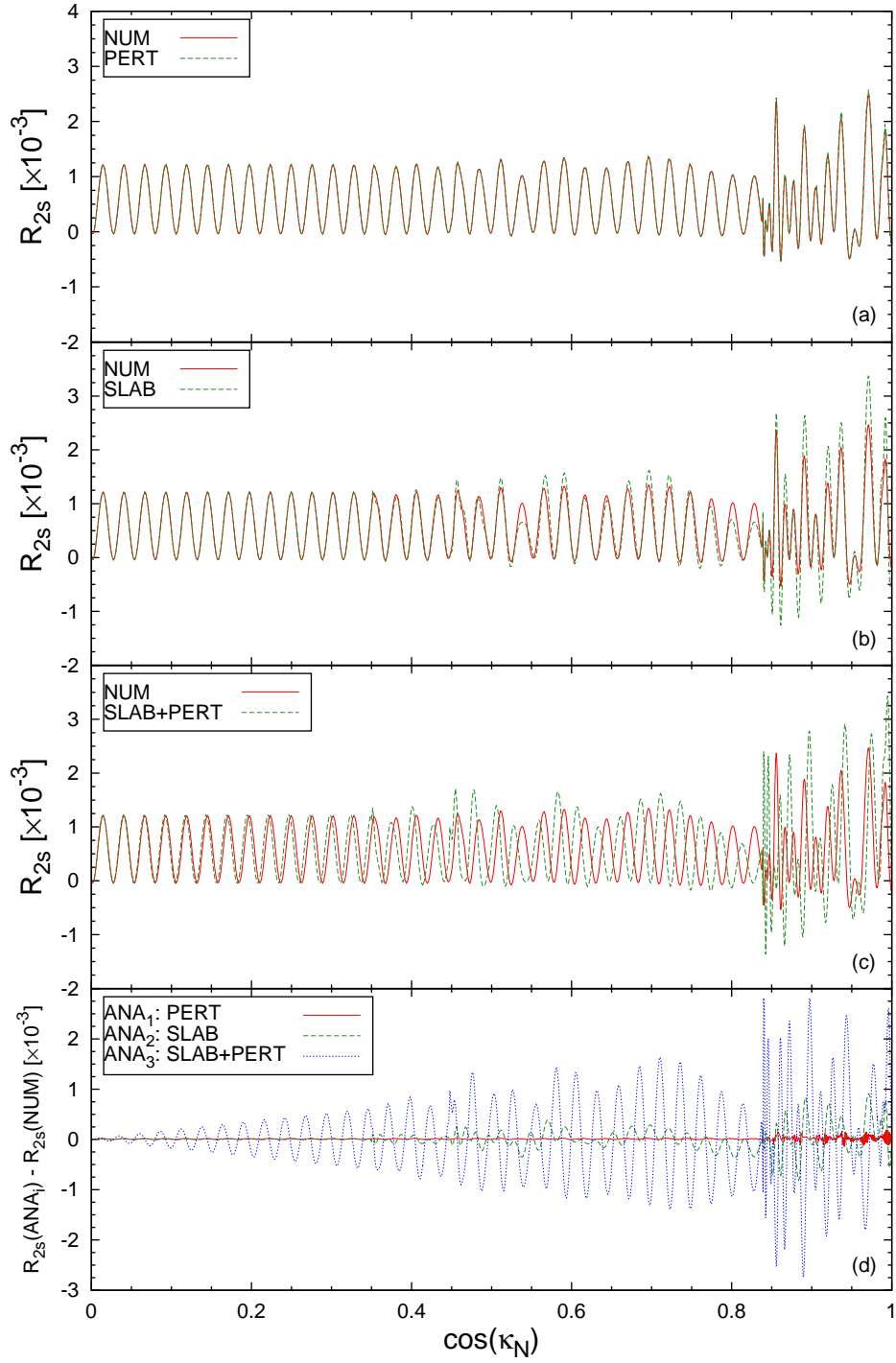


Figure 2: The same as Figure 1, but for the regeneration factor R_{2s} .

	Experimental Site	Latitude		Experimental Site	Latitude
1	Kamioka	36.42°N	4	Kaiping	22.15°N
2	Gran Sasso	42.46°N	5	Pyhasalmi	63.66°N
3	Sudbury	46.47°N	6	South Pole	90°S

Table 2: Latitudes of six experimental sites for three ongoing experiments (left) and three planned experiments (right).

will show later, these discrepancies are acceptable when the regeneration factors are averaged over the relevant ranges of the energy and/or nadir angle. Finally, one can notice that the accuracy of the SLAB+PERT approximation is low, both for the frequencies and the amplitudes of the oscillatory regeneration factors. Therefore, the SLAB+PERT approximation can be used only for a qualitative analysis and is not suitable for any realistic calculations.

The PERT approximation is the most accurate one, but it turns out to be very time-consuming because of the two-dimensional numerical integration in Eq. (49). Hence, in the data analysis of solar neutrino experiments it is convenient to employ the SLAB approximation, which gives a rapid and approximately accurate description for the terrestrial matter effect. In the following discussion, we use the SLAB approximation as our default choice.

The regeneration factors and the day-night asymmetries depend on the nadir angle κ_N of the incoming solar neutrinos, and thus on the latitude of the experimental site. With the aim of illustrating the dependence on the site latitude, we define the annual averaged quantity

$$\overline{Q}(E) = \frac{\int_{\kappa_N^{\min}}^{\kappa_N^{\max}} W(\kappa_N) Q(E, \kappa_N) d\kappa_N}{\int_{\kappa_N^{\min}}^{\kappa_N^{\max}} W(\kappa_N) d\kappa_N}, \quad (57)$$

where $Q = R_{2\beta}$ or $D_{e\beta}$, and the weight function $W(\kappa_N)$ represents the solar exposure of the trajectory and depends on the latitude of the experimental site. κ_N^{\max} and κ_N^{\min} are the possible maximal and minimal values of the nadir angle at a certain latitude (see Table II in Ref. [43]). In our calculation, we use the form of $W(\kappa_N)$ defined in Appendix C of Ref. [43], in order to illustrate the effect of the average over the nadir angle.

In the following we consider for illustration six experimental sites: three with ongoing neutrino experiments (Kamioka in Japan, Gran Sasso in Italy, and Sudbury in Canada) and three with planned neutrino experiments (Kaiping [44] in China, Pyhasalmi [45] in Finland, and the South Pole [46]). Their latitudes are listed in Table 2. The left and right panels in Fig. 3 show the behavior as a function of the neutrino energy E of the annual averages during the nighttime of the regeneration factors R_{2e} and R_{2s} calculated with the SLAB approximation for the six typical examples in Table 2. The oscillation parameters are set to M1 and P1 in Eqs. (96) and (97). One can see that the annual averages of the regeneration factors increase almost monotonously with the neutrino energy, except for tiny oscillatory variations.

The behavior of the averaged regeneration factors in Fig. 3 can be understood with the help of Eq. (54). The magnitudes of the regeneration factors are proportional to the

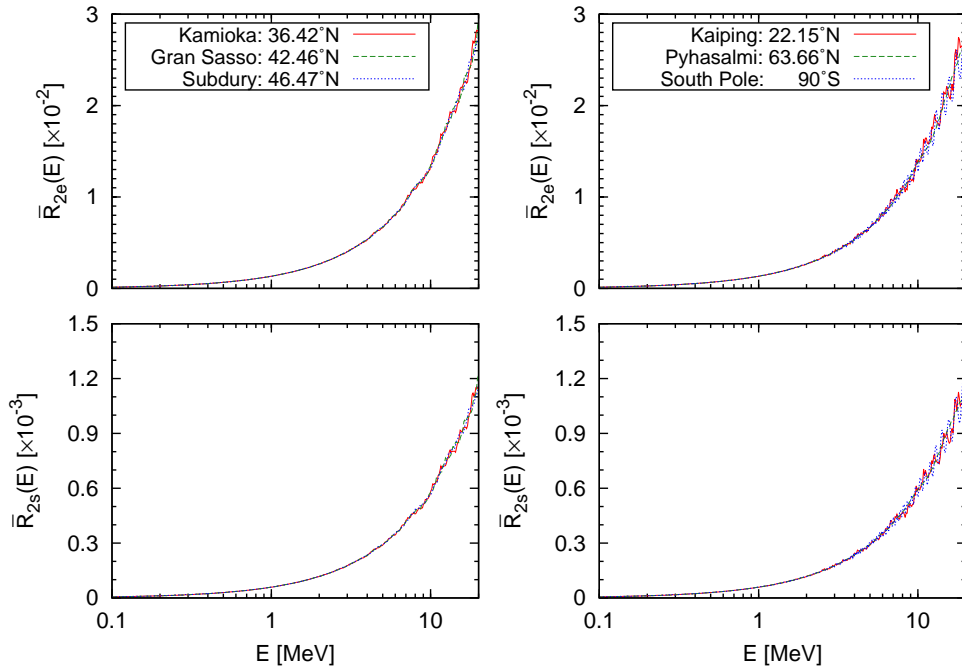


Figure 3: Annual averages of the regeneration factors over the nadir angle κ_N . The experimental site latitudes are selected for six typical examples in Table 2. All the oscillation parameters are set to M1 and P1 in Eqs. (96) and (97).

neutrino energy via the amplitude term V_k/δ , which contributes dominantly to the shape of the curves and determines the sizes of the regeneration factors. The residual oscillatory behavior is due to the summation of the functions $\sin(\delta L_n + \Phi_{\beta(k)})(\sin \delta L_k - \sin \delta L_{k-1})$ for $n \leq 5$ and $1 \leq k \leq n$, which oscillate as functions of the trajectory length, which is determined by the nadir angle. The averaging over the nadir angle reduces the size of the oscillation amplitudes. The size and pattern of the oscillatory behavior are different for different site latitudes, thus their effects are more significant in the right panels of Fig. 3, where the experimental sites range from the tropic area to the South Pole. In the following discussion, we consider only the Kamioka site for simplicity.

As we have illustrated in Figs. 1 and 2, the accuracy of the SLAB approximation is low for neutrinos crossing the core of the Earth when one considers precise values of the energy and nadir angle. Now we check the validity of the SLAB approximation in a more realistic case, in which the regeneration factors are averaged over bins of the nadir angle κ_N and the neutrino energy E . The annual average of the regeneration factor in the (i, j) bin is defined as

$$\overline{R}_{2\beta} = \frac{\int_{E_j^{\min}}^{E_j^{\max}} \int_{\kappa_{N_i}^{\min}}^{\kappa_{N_i}^{\max}} W(\kappa_N) W'(E) R_{2\beta}(E, \kappa_N) d\kappa_N dE}{\int_{\kappa_{N_i}^{\min}}^{\kappa_{N_i}^{\max}} W(\kappa_N) d\kappa_N \times \int_{E_j^{\min}}^{E_j^{\max}} W'(E) dE}, \quad (58)$$

where $W(\kappa_N)$ and $W'(E)$ are the weight functions of the nadir angle and neutrino energy. We use the expression of $W(\kappa_N)$ given in Appendix C of Ref. [43]. The weight function $W'(E)$ depends on the energy-dependent flux spectrum, the detection cross section and

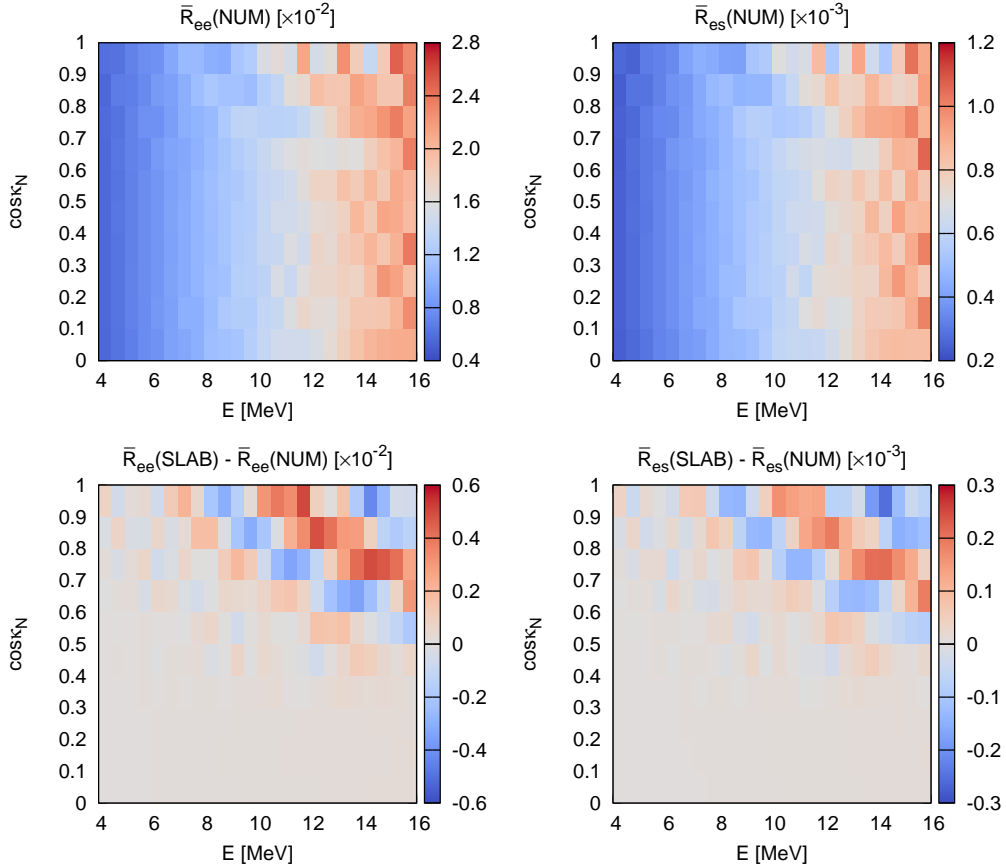


Figure 4: Binned average of the numerical (NUM) calculations (upper panels) of the regeneration factors R_{2e} (left) and R_{2s} (right) as the functions of the neutrino energy and the nadir angle. The lower panels illustrate the differences between the NUM and SLAB calculations. All the oscillation parameters are set to M1 and P1 in Eqs. (96) and (97).

the experimental efficiency. However, for simplicity we neglect the effect of $W'(E)$, since the energy bin-size is small compared to the variations of $W'(E)$.

In the upper panels of Fig. 4, we show the binned average of the numerical (NUM) calculations of the regeneration factors R_{2e} (left) and R_{2s} (right) as functions of the neutrino energy and nadir angle. The lower panels illustrate the corresponding differences between the NUM and SLAB calculations. All the oscillation parameters are set to M1 and P1 in Eqs. (96) and (97), and the latitude for the Kamioka site is assumed. In our calculation, we choose equal-sized bins for the neutrino energy ($\Delta E = 0.5$ MeV) and the cosine of the nadir angle ($\Delta \cos \kappa_N = 0.1$). From the lower panels of Fig. 4, we can observe that the discrepancy between the NUM and SLAB calculations of the regeneration factors is visible only for high neutrino energies and small nadir angles. The accuracy of the SLAB calculation of the binned average is excellent in most of the parameter space, and is better than 20% in the worst case. Thus, we conclude that the SLAB approximation is reliable for practical applications.

Next, we are going to explore the properties of the annual averages \bar{D}_{ee} and \bar{D}_{es} defined in Eq. (57) of the day-night asymmetries of solar neutrino oscillations defined in Eq. (39).

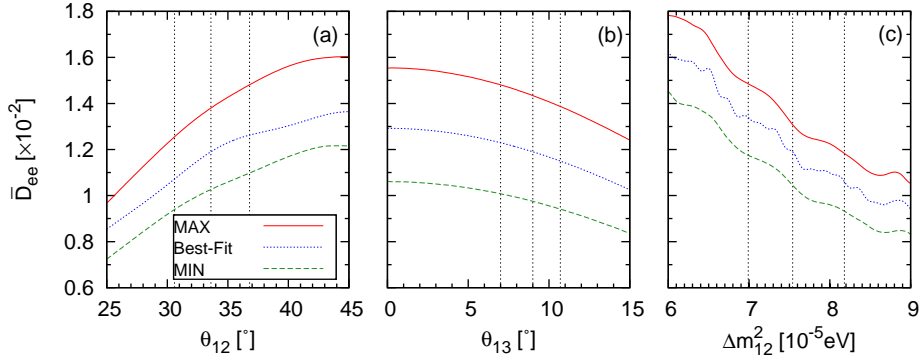


Figure 5: Dependence of \overline{D}_{ee} on the oscillation parameters θ_{12} (left), θ_{13} (middle) and Δm_{21}^2 (right) in the three-neutrino mixing scheme for $E = 10$ MeV and zero CP-violating phase. The solid and dashed lines in each panel correspond to the maximal (MAX) and minimal (MIN) values of \overline{D}_{ee} when the other parameters are scanned in the full $\pm 3\sigma$ ranges [47]. The short-dashed line corresponds to the best-fit values of these parameters. The three vertical lines in each panel correspond to the best-fit and $\pm 3\sigma$ values of the parameter in abscissa.

Although the regeneration factors $\overline{R}_{2\beta}(E)$ are always positive in the whole energy range, $\overline{D}_{e\beta}$ can be both positive or negative, depending on the sign of the parameter $\cos 2\Theta_e^0$. From the energy dependence of $\cos 2\Theta_e^0$ in Fig. 5 of Ref. [19], we know that the sign of $\cos 2\Theta_e^0$ flips at $E \simeq 2$ MeV and thus the sign of $\overline{D}_{e\beta}$ changes accordingly. For neutrino energies lower than about 2 MeV, both \overline{D}_{ee} and \overline{D}_{es} are negative and their magnitudes are of the order of 10^{-4} , which is too small for the detection ability of ongoing and near-future solar neutrino experiments. For neutrino energy greater than about 2 MeV, the day-night asymmetries increase monotonously as the energy grows, giving hope for their detection.

To illustrate the different contributions of the oscillation parameters to the day-night asymmetries, we first show in Figure 5 the dependence of \overline{D}_{ee} on the relevant oscillation parameters θ_{12} (left), θ_{13} (middle) and Δm_{21}^2 (right) in the three-neutrino mixing scheme for $E = 10$ MeV. The solid and dashed lines in each panel correspond to the maximal (MAX) and minimal (MIN) values of \overline{D}_{ee} when the other parameters (e.g. θ_{12} and θ_{13} in the right panel) are scanned in the full $\pm 3\sigma$ ranges [47]. The short-dashed line corresponds to the best-fit values of these parameters. The three vertical lines in each panel correspond to the best-fit and $\pm 3\sigma$ values of the parameter in abscissa. One can see that the magnitude of the day-night asymmetry is of the order of 10^{-2} . Moreover, one can see that \overline{D}_{ee} increases with θ_{12} , but decreases as θ_{13} increases. This can be explained with the help of Eqs. (84) and (86), which show that the day-night asymmetry is proportional to $\cos^4 \theta_{13} \sin^2 2\theta_{12}$. Considering the role of Δm_{21}^2 , higher Δm_{21}^2 induce lower values of \overline{D}_{ee} , which is consistent with the fact that the asymmetry is proportional to $1/\delta = 4E/\Delta m_{21}^2$ in Eq. (86).

Considering now the 3+1 mixing scheme, in Fig. 6 we illustrate the dependence of \overline{D}_{ee} (upper panels) and \overline{D}_{es} (lower panels) on the active neutrino oscillation parameters

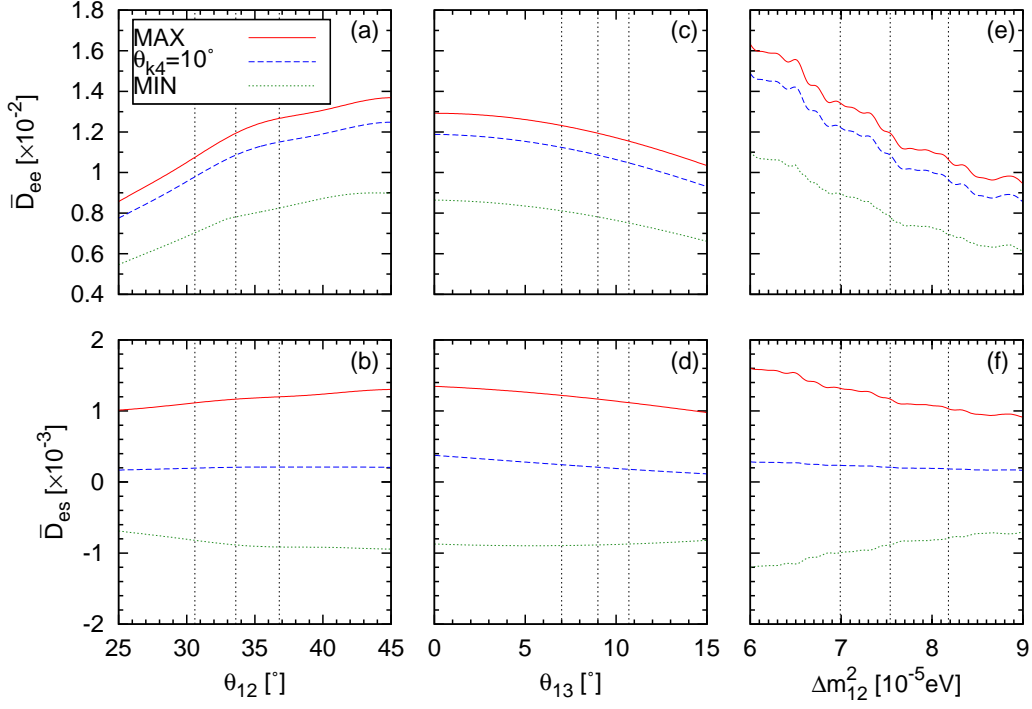


Figure 6: Dependence of \bar{D}_{ee} (upper panels) and \bar{D}_{es} (lower panels) on the active neutrino oscillation parameters θ_{12} (left), θ_{13} (middle) and Δm_{21}^2 (right) for $E = 10$ MeV and zero CP-violating phases. The solid and dashed lines correspond to the MAX and MIN values of \bar{D}_{ee} or \bar{D}_{es} when the active-sterile mixing angles θ_{k4} are scanned in the interval $[0^\circ, 20^\circ]$. The short-dashed lines correspond to $\theta_{k4} = 10^\circ$. The three vertical lines correspond to the best-fit and $\pm 3\sigma$ values of the parameter in abscissa. In each panel, the values of the other active neutrino oscillation parameters (e.g. θ_{13} and Δm_{21}^2 in the left panels) are fixed to their best-fit values [47].

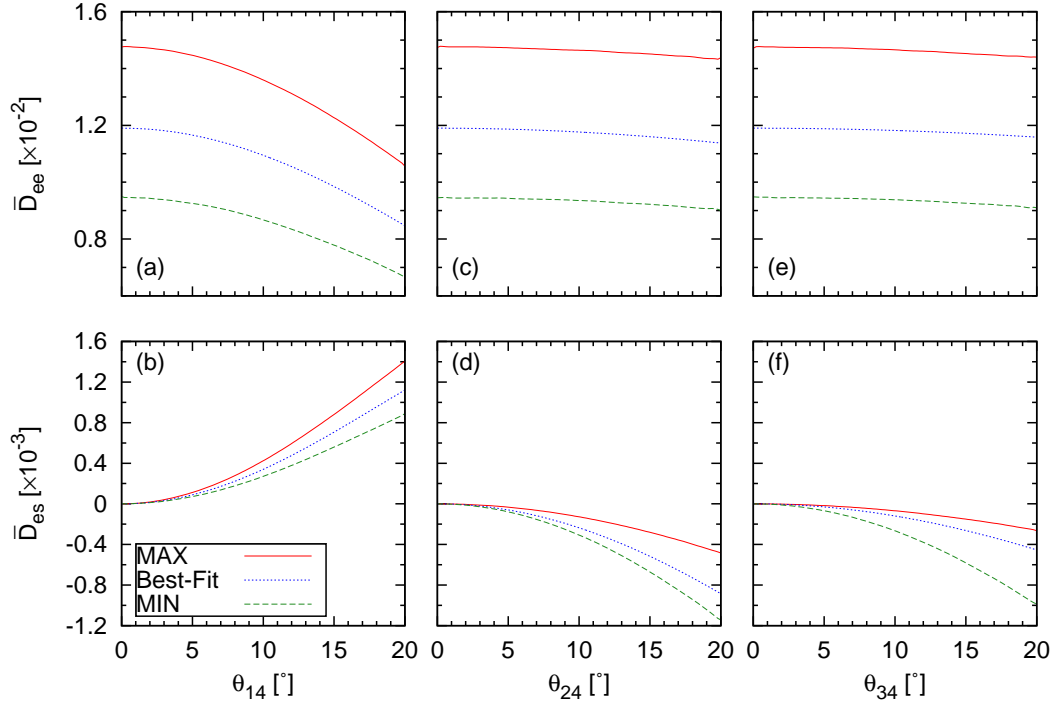


Figure 7: Dependence of \bar{D}_{ee} (upper panels) and \bar{D}_{es} (lower panels) on the active-sterile neutrino mixing parameters θ_{14} (left), θ_{24} (middle) and θ_{34} (right) for $E = 10$ MeV and zero CP-violating phases. The solid and dashed lines in each panel correspond to the MAX and MIN values of \bar{D}_{ee} or \bar{D}_{es} when the three active mixing angles are scanned in the full $\pm 3\sigma$ ranges [47]. The short-dashed line corresponds to the best-fit values of these parameters. In each panel the values of the other active-sterile mixing angles (e.g. θ_{14} and θ_{24} in the right panels) are fixed to be zero.

θ_{12} (left), θ_{13} (middle) and Δm_{21}^2 (right) for $E = 10$ MeV and zero CP-violating phases. The solid and dashed lines correspond to the MAX and MIN values of \overline{D}_{ee} or \overline{D}_{es} when the active-sterile mixing angles θ_{k4} are scanned in the interval $[0^\circ, 20^\circ]$. The short-dashed lines correspond to $\theta_{k4} = 10^\circ$. The three vertical lines correspond to the best-fit and $\pm 3\sigma$ values of the parameter in abscissa. In each panel, the values of the other active neutrino oscillation parameters (e.g. θ_{13} and Δm_{21}^2 in the left panels) are fixed to their best-fit values [47]. Similar illustrations are given in Fig. 7 for the active-sterile mixing parameters θ_{14} (left), θ_{24} (middle) and θ_{34} (right). The solid and dashed lines in each panel correspond to the MAX and MIN values of \overline{D}_{ee} or \overline{D}_{es} when the three active mixing angles are scanned in the full $\pm 3\sigma$ ranges [47]. The short-dashed line corresponds to the best-fit values of these parameters. In each panel the values of the other active-sterile mixing angles (e.g. θ_{14} and θ_{24} in the right panels) are fixed to be zero.

From the upper panels of Fig. 6, one can see that the dependence of \overline{D}_{ee} on θ_{12} , θ_{13} and Δm_{21}^2 is similar to that in the case of three neutrino mixing⁴, but the contributions of active-sterile mixing reduce the size of \overline{D}_{ee} . Moreover, we can observe from the upper panels of Fig. 7 that this suppression is mainly due to θ_{14} . This is explained by the presence of the factor $\cos^2 \chi_e = \cos^2 \theta_{13} \cos^2 \theta_{14}$ in Eq. (39), whereas the smallness of the effects of θ_{24} and θ_{34} on \overline{D}_{ee} is due to the fact that they only contribute indirectly through the parameters Θ_e^0 , V and ξ .

In the lower panels of Figs. 6 and 7, the magnitude of \overline{D}_{es} grows as the active-sterile mixing becomes larger, but the sign depends on the mixing angle: it is positive for the contribution of θ_{14} and negative for the contributions of θ_{24} and θ_{34} . Therefore, there are more possibilities to measure \overline{D}_{es} if θ_{14} is much larger than θ_{24} and θ_{34} or vice versa. In any case, high-precision experiments are needed, because the maximum value of \overline{D}_{es} is of the order of 10^{-3} .

Finally, it is interesting to investigate the effects of the three CP-violating phases on the day-night asymmetries \overline{D}_{ee} and \overline{D}_{es} . The left (right) panel of Figure 8 shows, as a function of the neutrino energy, the possible difference between the annually averaged day-night asymmetry $\overline{D}_{ee}(\eta)$ ($\overline{D}_{es}(\eta)$) obtained with non-zero CP-violating phases η_{13} , η_{24} , η_{34} and $\overline{D}_{ee}(0)$ ($\overline{D}_{es}(0)$) obtained with vanishing CP-violating phases. The MAX and MIN curves show, respectively, the maximal and minimal values of the difference which have been obtained with a random scan of all values of the CP-violating phases. Note that the values of the phases in each of these two curves may be different at different energies. From Fig. 8, we can learn that the effects of the CP-violating phases are negligible in the low energy region and start to emerge at about 2 MeV. Above this energy, the effects of the unknown CP-violating phases increase with the energy, reaching a maximum level of the order of 10^{-3} for $E \gtrsim 10$ MeV. Therefore, the relative variations of the day-night asymmetries due to the CP-violating phases can reach about 10% for \overline{D}_{ee} and may be as large as 100% for \overline{D}_{es} in the active-sterile transition. This conclusion is consistent with those on the oscillation probabilities in the daytime [19].

⁴ In the specific parametrization of U in Eq. (87), the day-night asymmetries depend also on the mixing angle θ_{23} due the non-commutativity of the matrices, but the dependence is negligible because of the smallness of the active-sterile mixing.

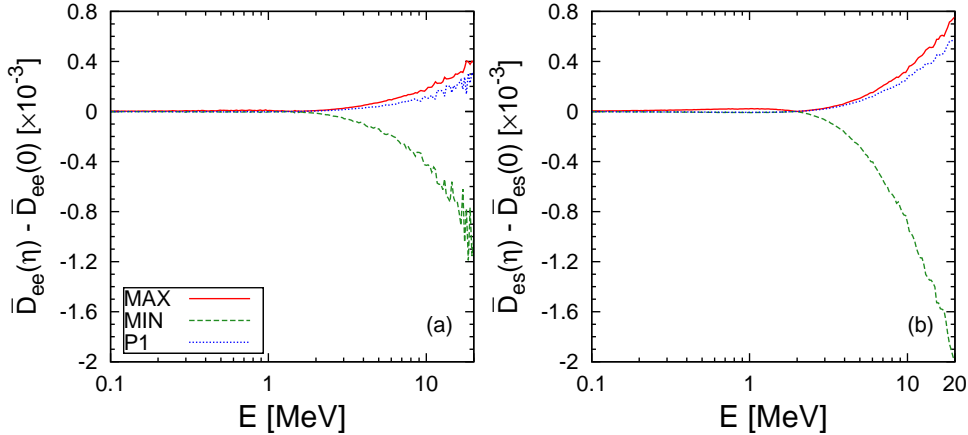


Figure 8: Energy spectra of the differences $\overline{D}_{e\beta}(\eta) - \overline{D}_{e\beta}(0)$ of the annually averaged day-night asymmetry $\overline{D}_{e\beta}(\eta)$ obtained with non-zero CP-violating phases and $\overline{D}_{e\beta}(0)$ obtained with vanishing CP-violating phases. The mass and mixing parameters are set to M1 in Eq. (96). The three CP-violating phases η_{13} , η_{24} , η_{34} have been randomly scanned in the full parameter space to produce the MAX and MIN boundary curves. The short-dashed curve corresponds to the set of phases P1 in Eq. (97).

5 Conclusion

In this paper, we have discussed solar neutrino oscillations inside the Earth and we have derived the regeneration factors (38) and the day-night asymmetries (39) of solar neutrino oscillations in a general scheme of $3+N_s$ neutrino mixing, without any constraint on the neutrino mixing elements, assuming only a realistic hierarchy on the mass-squared differences. We have discussed two approximate analytical solutions of the neutrino evolution inside the Earth, the perturbative approximation and the slab approximation, which allow us to calculate the regeneration factors and the day-night asymmetries with different accuracy levels and computational burdens.

In Section 4 we have presented several examples of numerical calculations of solar neutrino active-sterile oscillations inside the Earth in the $3+1$ neutrino mixing scheme. By using a simplified version of the PREM description of the Earth density profile, we tested the analytical approximations and learned that the perturbative approximation can give the most accurate description of the neutrino evolution inside the Earth and the slab approximation gives less accurate but more efficient calculations.

We have shown that the annual averages \overline{D}_{ee} and \overline{D}_{es} of the $\nu_e \rightarrow \nu_e$ and $\nu_e \rightarrow \nu_s$ day-night asymmetries are insensitive to the latitude differences of the experimental sites and increase with the neutrino energy. The magnitudes of \overline{D}_{ee} and \overline{D}_{es} can reach, respectively, a size of the order of 10^{-2} and 10^{-3} for high-energy solar neutrinos. The three active-sterile mixing angles θ_{14} , θ_{24} and θ_{34} have a suppression effect on \overline{D}_{ee} (mostly θ_{14}). Studying the dependence of \overline{D}_{es} on the active-sterile mixing angles, we found that the active-sterile mixing angle θ_{14} generates a positive contribution to \overline{D}_{es} , whereas the contribution of θ_{24} and θ_{34} is negative. Therefore, there are more possibilities to measure \overline{D}_{es} if θ_{14} is much larger than θ_{24} and θ_{34} or vice versa. Finally, we have shown that the variations

of the annual averages \overline{D}_{ee} and \overline{D}_{es} induced by the unknown CP-violating phases can be at the level of 10^{-3} in the high energy region. Therefore, it might be possible to observe the effects of active-sterile mixing and that of the CP-violating phases in the day-night asymmetries in future high-precision solar neutrino experiments.

Acknowledgment

H.W. L. would like to thank Prof. Peng-Fei Zhang for his continuous encouragement and financial support. The work of H.W. L. is supported in part by the National Natural Science Foundation of China under Grant No. 11265006. The work of Y. F. L. is supported in part by the National Natural Science Foundation of China under Grant No. 11135009.

A Details of the Analytical Calculation

Since the S -matrix of the neutrino evolution in the Earth defined in Eq. (41) is a 2×2 unitary matrix, we can rewrite S^V using the Pauli matrices,

$$\begin{aligned} S^V &= Q_0 \cdot \mathbf{1} - i\vec{\sigma} \cdot \vec{Q} \\ &= Q_0 \cdot \mathbf{1} - i(Q_1 \cdot \sigma_1 + Q_2 \cdot \sigma_2 + Q_3 \cdot \sigma_3) \quad . \end{aligned} \quad (59)$$

Then from Eqs. (40) and (41), and the initial condition, we have

$$\begin{aligned} P_{\nu_2 \rightarrow \nu_\beta}^E(x_f) &= \frac{1}{2} \cos^2 \chi_\beta \left\{ 1 + \cos 2\theta_\beta (Q_1^2 + Q_2^2 - Q_3^2 - Q_0^2) \right. \\ &\quad - 2 \sin 2\theta_\beta \cos(\phi_{\beta 2} - \phi_{\beta 1}) (Q_0 Q_2 + Q_1 Q_3) \\ &\quad \left. - 2 \sin 2\theta_\beta \sin(\phi_{\beta 2} - \phi_{\beta 1}) (Q_0 Q_1 - Q_2 Q_3) \right\} \quad . \end{aligned} \quad (60)$$

All the following calculations are based on this expression.

A.1 Perturbative Approximation

Comparing Eqs. (43) and (59), we can get the expressions of Q_i in the perturbative approximation as

$$\begin{aligned} Q_0 &= \cos \Delta - A \sin \Delta , \\ Q_1 &= \operatorname{Re}(C) \cos \Delta - \operatorname{Im}(C) \sin \Delta , \\ Q_2 &= -\operatorname{Re}(C) \sin \Delta - \operatorname{Im}(C) \cos \Delta , \\ Q_3 &= -\sin \Delta - A \cos \Delta \quad . \end{aligned} \quad (61)$$

According to Eq. (60) and to the first order of A and C , we obtain

$$\begin{aligned} P_{\nu_2 \rightarrow \nu_\beta}^E(x_f) &\simeq P_{\nu_2 \rightarrow \nu_\beta}^V + \cos^2 \chi_\beta \sin 2\theta_\beta \times \\ &\quad [\operatorname{Re}(C) \sin(2\Delta + \phi_{\beta 1} - \phi_{\beta 2}) + \operatorname{Im}(C) \cos(2\Delta + \phi_{\beta 1} - \phi_{\beta 2})] \quad , \end{aligned} \quad (62)$$

which leads to Eq. (48).

The electron fraction Y_e can be approximated as constant in the Earth, so we can further simplify the corresponding term of C as

$$\begin{aligned} \operatorname{Im}[C e^{i(2\Delta + \phi_{\beta 1} - \phi_{\beta 2})}] &= \int_{x_i}^{x_f} -\dot{\omega} \cos[2\Delta(x_f, x) + \Phi_\beta] dx \\ &= -\omega \cos[2\Delta(x_f, x) + \Phi_\beta] \Big|_{x_i}^{x_f} + \int_{x_i}^{x_f} \omega \delta_M \sin[2\Delta(x_f, x) + \Phi_\beta] dx \quad , \end{aligned} \quad (63)$$

where $\Phi_\beta = \phi_{\beta 1} - \phi_{\beta 2} + \varphi$.

Since $\omega(x_i) = 0$, $\Delta(x_f, x_f) = 0$ and to the first order of V

$$\omega \simeq \frac{\sin 2\xi}{2\delta} V \quad , \quad \delta_M \simeq \delta - \cos 2\xi \cdot V \quad , \quad (64)$$

we obtain the perturbative approximation of $P_{\nu_2 \rightarrow \nu_\beta}^E(x_f)$ in Eq. (49).

A.2 Slab Approximation

To calculate the transition probability $P_{\nu_2 \rightarrow \nu_\beta}^E$ in the slab approximation, it is useful to rewrite S_{slab}^V and S_k^V in Eq. (53) in terms of the Pauli matrices. First, for S_k^V we have

$$\begin{aligned} S_k^V &= [W(\omega, \varphi) S_{\text{ad}}^M(\Delta x_k) W^\dagger(\omega, \varphi)]_{(k)} \\ &= c_k \cdot \mathbf{1} - i\vec{\sigma} \cdot \vec{s}_k \quad , \end{aligned} \quad (65)$$

with

$$c_k \equiv \cos \eta_k \quad , \quad (66)$$

$$\vec{s}_k \equiv \sin \eta_k (\sin 2\omega_k \cos \varphi_k, -\sin 2\omega_k \sin \varphi_k, -\cos 2\omega_k) \quad , \quad (67)$$

$$\eta_k \equiv \delta_{M(k)} \Delta x_k \quad . \quad (68)$$

Then, we can define

$$S_{\text{slab}(k)}^V = c'_k \cdot \mathbf{1} - i\vec{\sigma} \cdot \vec{s}'_k \quad (69)$$

with

$$S_{\text{slab}(k)}^V = S_k^V S_{\text{slab}(k-1)}^V S_k^V \quad , \quad (70)$$

$$S_{\text{slab}(0)}^V = \mathbf{1} \quad . \quad (71)$$

Therefore, we obtain

$$\begin{cases} c'_k &= c'_{k-1} (2c_k^2 - 1) - \vec{s}'_{k-1} \cdot (2c_k \vec{s}_k) \quad , \\ \vec{s}'_k &= c'_{k-1} (2c_k \vec{s}_k) - 2(\vec{s}'_{k-1} \cdot \vec{s}_k) \vec{s}_k + \vec{s}'_{k-1} \quad , \\ c'_0 &= 1 \quad , \\ \vec{s}'_0 &= (0, 0, 0) \quad , \end{cases} \quad (72)$$

or, in matrix form,

$$(c'_k, \vec{s}'_k) = (c'_{k-1}, \vec{s}'_{k-1}) T_k = (1, 0, 0, 0) \prod_{i=1}^k T_i \quad . \quad (73)$$

Here T_k is the 4×4 matrix

$$\begin{aligned} T_k &= \begin{pmatrix} 2c_k^2 - 1 & 2c_k \vec{s}_k \\ -2c_k \vec{s}_k^T & \mathbf{1} - 2\vec{s}_k \otimes \vec{s}_k \end{pmatrix} = \\ &= \begin{pmatrix} \cos 2\eta & \cos \varphi \sin 2\eta \sin 2\omega & -\sin \varphi \sin 2\eta \sin 2\omega & -\sin 2\eta \cos 2\omega \\ -\cos \varphi \sin 2\eta \sin 2\omega & 1 - 2\cos^2 \varphi \sin^2 \eta \sin^2 2\omega & \sin 2\varphi \sin^2 \eta \sin^2 2\omega & \cos \varphi \sin^2 \eta \sin 4\omega \\ \sin \varphi \sin 2\eta \sin 2\omega & \sin 2\varphi \sin^2 \eta \sin^2 2\omega & 1 - 2\sin^2 \varphi \sin^2 \eta \sin^2 2\omega & -\sin \varphi \sin^2 \eta \sin 4\omega \\ \sin 2\eta \cos 2\omega & \cos \varphi \sin^2 \eta \sin 4\omega & -\sin \varphi \sin^2 \eta \sin 4\omega & 1 - 2\cos^2 2\omega \sin^2 \eta \end{pmatrix} \quad , \end{aligned} \quad (74)$$

where the subscripts (k) and k denote the quantities in the $(N-n+k)$ -th shell. Finally, we obtain the following compact expression for S_{slab}^V which allows to calculate the evolution of the amplitudes in the Earth according to Eq. (52):

$$S_{\text{slab}}^V = (\mathbf{1}, -i\vec{\sigma}) \cdot (c'_n, \vec{s}'_n) = (\mathbf{1}, -i\vec{\sigma}) \cdot \left[(1, 0, 0, 0) \prod_{i=1}^n T_i \right] \quad . \quad (75)$$

This expression corresponds to that in Eq. (59) with

$$Q_j = \left(\prod_{i=1}^n T_i \right)_{0j}, \quad \text{for } j = 0, 1, 2, 3, \quad (76)$$

and allows to calculate $P_{\nu_2 \rightarrow \nu_\beta}^E(x_n) = P_{\nu_2 \rightarrow \nu_\beta}^E(x_f)$ through Eq. (60).

Let us now derive the perturbative approximation in Eq. (54). To the first order of V_k , we can approximate T_k by

$$T_k \simeq T_k^0 + J_k \cdot V_k, \quad (77)$$

where

$$\begin{aligned} T_k^0 &= R_{14}^\dagger(2\eta_{0(k)}) = R_{14}^\dagger(2\delta\Delta x_k) \\ &= \begin{pmatrix} \cos(2\delta\Delta x_k) & 0 & 0 & -\sin(2\delta\Delta x_k) \\ 0 & 1 & 0 & 0 \\ 0 & 0 & 1 & 0 \\ \sin(2\delta\Delta x_k) & 0 & 0 & \cos(2\delta\Delta x_k) \end{pmatrix}, \end{aligned} \quad (78)$$

and

$$J_k = \begin{pmatrix} 2 \cos 2\xi \sin(2\delta\Delta x) \Delta x & \frac{\sin 2\xi \cos \varphi \sin(2\delta\Delta x)}{\delta} & -\frac{\sin 2\xi \sin \varphi \sin(2\delta\Delta x)}{\delta} & 2 \cos 2\xi \cos(2\delta\Delta x) \Delta x \\ -\frac{\sin 2\xi \cos \varphi \sin(2\delta\Delta x)}{\delta} & 0 & 0 & \frac{2 \sin 2\xi \cos \varphi \sin^2(\delta\Delta x)}{\delta} \\ \frac{\sin 2\xi \sin \varphi \sin(2\delta\Delta x)}{\delta} & 0 & 0 & -\frac{2 \sin 2\xi \sin \varphi \sin^2(\delta\Delta x)}{\delta} \\ -2 \cos 2\xi \cos(2\delta\Delta x) \Delta x & \frac{2 \sin 2\xi \cos \varphi \sin^2(\delta\Delta x)}{\delta} & -\frac{2 \sin 2\xi \sin \varphi \sin^2(\delta\Delta x)}{\delta} & 2 \cos 2\xi \sin(2\delta\Delta x) \Delta x \end{pmatrix}^{(k)}. \quad (79)$$

Then we have

$$\begin{aligned} \prod_{k=1}^n T_k &\simeq \prod_{k=1}^n (T_k^0 + J_k \cdot V_k) \\ &\simeq \prod_{k=1}^n T_k^0 + \sum_{k=1}^n \left[\left(\prod_{i=1}^{k-1} T_i^0 \right) J_k \left(\prod_{j=k+1}^n T_j^0 \right) \right] V_k \\ &= R_{14}^\dagger(\delta L_n) + \sum_{k=1}^n \left[R_{14}^\dagger(\delta L_{k-1}) J_k R_{14}^\dagger(\delta(L_n - L_k)) \right] V_k, \end{aligned} \quad (80)$$

with L_k defined in Eq. (55). According to Eq. (75), we only need to calculate the first row of the 4×4 matrix, whose elements are

$$\begin{aligned} Q_0 &= \cos \delta L_n + 2 \sin \delta L_n \sum_{k=1}^n \cos 2\xi_k \cdot \Delta x_k V_k \\ Q_1 &= 2 \sum_{k=1}^n \sin 2\xi_k \cos \varphi_k \cos \delta(L_{k-1} + \Delta x_k) \sin(\delta\Delta x_k) \cdot \frac{V_k}{\delta} \end{aligned}$$

$$\begin{aligned}
Q_2 &= -2 \sum_{k=1}^n \sin 2\xi_k \sin \varphi_k \cos \delta(L_{k-1} + \Delta x_k) \sin(\delta \Delta x_k) \cdot \frac{V_k}{\delta} \\
Q_3 &= -\sin \delta L_n + 2 \cos \delta L_n \sum_{k=1}^n \cos 2\xi_k \cdot \Delta x_k V_k \quad .
\end{aligned} \tag{81}$$

Finally, from Eq. (60), we obtain the approximation in Eq. (54) of $P_{\nu_2 \rightarrow \nu_\beta}^E(x_n)$ up to the first order of V .

A.3 Three-Neutrino mixing

In this subsection we derive the limits of the expressions for $P_{\nu_2 \rightarrow \nu_e}^E$ that we have obtained in Eq. (49) in the perturbative approximation and in Eq. (54) in the perturbative slab approximation for a check of consistency with those derived, respectively, in Refs. [35] and [34].

For $N_s = 0$ and $\beta = e$, within standard parameterization [6] of the mixing matrix, we have

$$\theta_e = \theta_{12}, \quad \chi_e = \theta_{13}, \quad \phi_{e1} = \phi_{e2} = \varphi = 0, \tag{82}$$

and therefore

$$\xi = \theta_{12}, \quad V = \frac{1}{2} \cos^2 \theta_{13} V_{CC}, \quad P_{\nu_2 \rightarrow \nu_\beta}^V = \cos^2 \theta_{13} \sin^2 \theta_{12}. \tag{83}$$

For the perturbative approximation, we have

$$P_{\nu_2 \rightarrow \nu_e}^E(x_f) = P_{\nu_2 \rightarrow \nu_e}^V + \frac{\cos^4 \theta_{13} \sin^2 2\theta_{12}}{2} \int_{x_i}^{x_f} V_{CC}(x) \sin(2\Delta(x_f, x)) dx \quad , \tag{84}$$

where $\Delta(x_f, x)$ is given by Eq. (45) with

$$\delta_M = \sqrt{\left(\frac{1}{2} \cos^2 \theta_{13} V_{CC}(x) - \delta \cos 2\theta_{12}\right)^2 + (\delta \sin 2\theta_{12})^2} \quad . \tag{85}$$

For the slab approximation up to the first order of V_{CC} , we have

$$P_{\nu_2 \rightarrow \nu_e}^E(x_n) = P_{\nu_2 \rightarrow \nu_e}^V + \frac{\cos^4 \theta_{13} \sin^2 2\theta_{12} \sin(\delta L_n)}{2\delta} \sum_{k=1}^n (\sin \delta L_k - \sin \delta L_{k-1}) V_{CC(k)}. \tag{86}$$

The expressions in Eqs. (84) and (86) are consistent, respectively, with those in Refs. [35] and [34].

B Parametrization of U

The neutrino mixing matrix U for the 3+1 mixing scheme can be parametrized as the extension of the parametrization [6] for three-neutrino mixing

$$U = W^{34} W^{24} R^{14} R^{23} W^{13} R^{12} \quad , \tag{87}$$

with $W^{ab} = W(\theta_{ab}, \eta_{ab})$ being the complex unitary matrix in the (a, b) plane defined by

$$[W(\theta_{ab}, \eta_{ab})]_{rs} = \delta_{rs} + (\cos \theta_{ab} - 1)(\delta_{ra}\delta_{sa} + \delta_{rb}\delta_{sb}) \\ + \sin \theta_{ab}(e^{-i\eta_{ab}}\delta_{ra}\delta_{sb} - e^{i\eta_{ab}}\delta_{rb}\delta_{sa}) \quad , \quad (88)$$

where θ_{ab} and η_{ab} are the mixing angles and Dirac CP-violating phases. The real unitary matrix R^{ab} can be obtained by setting η_{ab} to be zero in W^{ab} .

In this parametrization, we can write down the explicit expressions for the electron and sterile rows of the mixing matrix U :

$$U_{e1} = c_{12}c_{13}c_{14} \quad , \quad U_{e2} = s_{12}c_{13}c_{14} \quad , \quad (89)$$

$$U_{e3} = s_{13}e^{-i\eta_{13}}c_{14} \quad , \quad U_{e4} = s_{14} \quad , \quad (90)$$

$$U_{s1} = -s_{14}c_{12}c_{13}c_{24}c_{34} + (s_{12}c_{23} + s_{13}e^{i\eta_{13}}s_{23}c_{12})s_{24}e^{i\eta_{24}}c_{34} \\ + (-s_{12}s_{23} + s_{13}e^{i\eta_{13}}c_{12}c_{23})s_{34}e^{i\eta_{34}} \quad , \quad (91)$$

$$U_{s2} = -s_{12}s_{14}c_{13}c_{24}c_{34} + (-c_{12}c_{23} + s_{12}s_{13}e^{i\eta_{13}}s_{23})s_{24}e^{i\eta_{24}}c_{34} \\ + (s_{23}c_{12} + s_{12}s_{13}e^{i\eta_{13}}c_{23})s_{34}e^{i\eta_{34}} \quad , \quad (92)$$

$$U_{s3} = -s_{13}e^{-i\eta_{13}}s_{14}c_{24}c_{34} - (s_{34}e^{i\eta_{34}}c_{23} + s_{23}s_{24}e^{i\eta_{24}}c_{34})c_{13} \quad , \quad (93)$$

$$U_{s4} = c_{14}c_{24}c_{34} \quad . \quad (94)$$

Moreover, we have

$$U_{\mu 4} = c_{14}s_{24}e^{-i\eta_{24}} \quad , \quad U_{\tau 4} = c_{14}c_{24}s_{34}e^{-i\eta_{34}} \quad . \quad (95)$$

We choose the following typical values for the oscillation parameters as

$$\text{M1 : } \begin{cases} \Delta m_{12}^2 \simeq 7.54 \times 10^{-5} \text{ eV} \\ \theta_{12} \simeq 33.6^\circ \\ \theta_{23} \simeq 39.1^\circ \\ \theta_{13} \simeq 9.0^\circ \\ \theta_{14} = \theta_{24} = \theta_{34} = 10^\circ \quad , \end{cases} \quad (96)$$

and

$$\text{P1 : } \quad \eta_{13} = 35^\circ \quad , \quad \eta_{24} = 75^\circ \quad , \quad \eta_{34} = 115^\circ \quad , \quad (97)$$

where the three mixing angles (θ_{12} , θ_{13} and θ_{23}) and Δm_{12}^2 , equivalent to the active neutrino oscillation parameters for three-neutrino mixing, are taken from the global analysis [47], the three mixing angles between the active and sterile flavors (θ_{14} , θ_{24} and θ_{34}) are motivated by the anomalies in the SBL data [7–11] and the non-trivial phases are selected to illustrate the effects of the CP-violating phases.

References

- [1] Daya Bay Collaboration, (F.P. An *et al.*), Phys. Rev. Lett. **108**, 171803 (2012).
- [2] Double Chooz Collaboration, (Y. Abe *et al.*), Phys. Rev. Lett. **108**, 131801 (2012).
- [3] RENO Collaboration, (J.K. Ahn *et al.*), Phys. Rev. Lett. **108**, 191802 (2012).
- [4] T2K Collaboration, (K. Abe *et al.*), Phys. Rev. Lett. **107**, 041801 (2011).
- [5] MINOS Collaboration, (P. Adamson *et al.*), Phys. Rev. Lett. **107**, 181802 (2011).
- [6] Particle Data Group, (K. Nakamura *et al.*), J. Phys. G **37**, 075021 (2010).
- [7] LSND Collaboration, (A. Aguilar *et al.*), Phys. Rev. D **64**, 112007 (2001).
- [8] MiniBooNE Collaboration, (A.A. Aguilar-Arevalo *et al.*), Phys. Rev. Lett. **105**, 181801 (2010).
- [9] G. Mention *et al.*, Phys. Rev. D **83**, 073006 (2011); P. Huber, Phys. Rev. C **84**, 024617 (2011).
- [10] C. Giunti and M. Laveder, Phys. Rev. C **83**, 065504 (2011).
- [11] C. Giunti, M. Laveder, Y.F. Li, Q.Y. Liu and H.W. Long, Phys. Rev. D **86**, 113014 (2012); C. Giunti, M. Laveder, Y.F. Li and H.W. Long, Phys. Rev. D **87**, 013004 (2013).
- [12] J. Kopp, M. Maltoni and T. Schwetz, Phys. Rev. Lett. **107**, 091801 (2011); J. Kopp, P. A.N. Machado, M. Maltoni and T. Schwetz, JHEP **1305**, 050 (2013).
- [13] C. Giunti and M. Laveder, Phys. Rev. D **84**, 073008 (2011); Phys. Rev. D **84**, 093006 (2011).
- [14] K.N. Abazajian *et al.*, (2012) arXiv:1204.5379 [hep-ph].
- [15] J. Hamann *et al.*, Phys. Rev. Lett. **105**, 181301 (2010); E. Giusarma *et al.*, Phys. Rev. D **83**, 115023 (2011); A.X. Gonzalez-Morales *et al.*, arXiv:1106.5052 [astro-ph.CO]; J. Hamann, JCAP **1203**, 021 (2012).
- [16] M. Archidiacono *et al.*, Phys. Rev. D **86**, 065028 (2012); arXiv:1302.6720.
- [17] G. Mangano and P.D. Serpico, Phys. Lett. B **701**, 296 (2011); J. Hamann *et al.*, JCAP **1109**, 034 (2011).
- [18] C. Giunti and Y.F. Li, Phys. Rev. D **80**, 113007 (2009); Prog. Part. Nucl. Phys. **64** 213 (2010).
- [19] H.W. Long, Y.F. Li and C. Giunti, Phys. Rev. D **87**, 113004 (2013).
- [20] A. Palazzo, Phys. Rev. D **83**, 113013 (2011).
- [21] A. Palazzo, Phys. Rev. D **85**, 077301 (2012).

- [22] P.C. de Holanda and A.Y. Smirnov, Phys. Rev. D **69**, 113002 (2004); Phys. Rev. D **83**, 113011 (2011).
- [23] S. Razzaque and A.Y. Smirnov JHEP **1107**, 084 (2011); V. Barger, Y. Gao and D. Marfatia, Phys. Rev. D **85**, 011302 (2012); A. Esmaili, F. Halzen and O. L. G. Peres, JCAP **1211**, 041 (2012).
- [24] A.I. Belesev *et al.*, JETP Lett. **97**, 67 (2013); C. Kraus, A. Singer, K. Valerius and C. Weinheimer, Eur. Phys. J. C **73**, 2323 (2013).
- [25] A.S. Riis and S. Hannestad, JCAP **1102**, 011 (2011); J.A. Formaggio and J. Barrett, Phys. Lett. B **706**, 68 (2011); A. Esmaili and O. L. G. Peres, Phys. Rev. D **85**, 117301 (2012).
- [26] C. Giunti and M. Laveder, Phys. Rev. D **82**, 053005 (2010); C. Giunti and M. Laveder, Phys. Lett. B **706**, 200 (2011); J. Barry *et al.*, JHEP **1107**, 091 (2011); Y.F. Li and S.S. Liu, Phys. Lett. B **706**, 406 (2012).
- [27] L. Wolfenstein, Phys. Rev. **D17**, 2369 (1978).
- [28] S.P. Mikheev and A.Y. Smirnov, Sov. J. Nucl. Phys. **42**, 913 (1985).
- [29] SNO Collaboration, (Q.R. Ahmad *et al.*), Phys. Rev. Lett. **89**, 011301 (2002).
- [30] KamLAND Collaboration, (K. Eguchi *et al.*), Phys. Rev. Lett. **90**, 021802 (2003).
- [31] Borexino Collaboration, (G. Bellini *et al.*), Phys. Rev. Lett. **107**, 141302 (2011); Phys. Rev. Lett. **108**, 051302 (2012).
- [32] E.D. Carlson, Phys. Rev. D **34**, 1454 (1986); A.J. Baltz and J. Weneser, Phys. Rev. D **35**, 528 (1987).
- [33] M. Blennow, T. Ohlsson and H. Snellman, Phys. Rev. D **69**, 073006 (2004).
- [34] E.Kh. Akhmedov, M.A. Tortola and J.W.F. Valle, JHEP **0405**, 057 (2004).
- [35] P.C. de Holanda, W. Liao and A.Yu. Smirnov, Nucl. Phys. B **702**, 307 (2004); W. Liao, Phys. Rev. D **77**, 053002 (2008).
- [36] S.S. Aleshin, O.G. Kharlanov and A.E. Lobanov, Phys. Rev. D **87**, 045025 (2013).
- [37] A.S. Dighe, Q.Y. Liu and A.Y. Smirnov, arXiv:hep-ph/9903329.
- [38] D. Dooling, C. Giunti, K. Kang and C. W. Kim, Phys. Rev. D **61**, 073011 (2000).
- [39] C. Giunti, M. C. Gonzalez-Garcia and C. Pena-Garay, Phys. Rev. D **62**, 013005 (2000).
- [40] E.K. Akhmedov, R. Johansson, M. Lindner, T. Ohlsson and T. Schwetz, JHEP **0404**, 078(2004).

- [41] A.N. Ioannisian and A.Yu. Smirnov, Phys. Rev. Lett. **93**, 241801 (2004); A.N. Ioannisian, N.A. Kazarian, A.Yu. Smirnov and D. Wyler, Phys. Rev. D **71**, 033006 (2005).
- [42] A.M. Dziewonski and D.L. Anderson, Phys. Earth Planet. Inter. **25**, 297 (1981).
- [43] E. Lisi, D. Montanino, Phys. Rev. D **56**, 1792 (1997).
- [44] Y.F. Li, J. Cao, Y.F. Wang and L. Zhan, Phys. Rev. D **88**, 013008 (2013).
- [45] LENA Collaboration, (M. Wurm *et al.*), Astropart. Phys. **35**, 685 (2012).
- [46] IceCube Collaboration, (R. Abbasi *et al.*), Astron. Astrophys. **535**, A109 (2011).
- [47] G.L. Fogli, E. Lisi, A. Marrone, D. Montanino, A. Palazzo and A.M. Rotunno, Phys. Rev. D **86**, 013012 (2012).